Electronic Supplementary Material (ESI) for Journal of Materials Chemistry A.

Supporting Information

Local microenvironment tuning induces switching between electrochemical CO_2 reduction pathways

Surani Bin Dolmanan[1,†], Annette Boehme[2,3,†], Ziting Fan[4,5,6,†], Alex J. King[7,8], Aidan Q. Fenwick[2,9], Albertus Denny Handoko[1], Wan Ru Leow[10], Adam Z. Weber[7,8], Xinbin Ma[4,5], Edwin Khoo[11], Harry A. Atwater[2,3]* and Yanwei Lum[1,6]*.

[1]Institute of Materials Research and Engineering, Agency for Science, Technology and Research (A*STAR), Innovis, Singapore.

[2]Liquid Sunlight Alliance, California Institute of Technology, Pasadena, California, United States

[3]Department of Applied Physics and Material Science, California Institute of Technology, Pasadena, California, United States

[4]Joint School of National University of Singapore and Tianjin University, International Campus of Tianjin University, Binhai New City, Fuzhou, China

[5]Key Laboratory for Green Chemical Technology of Ministry of Education, Collaborative Innovation Center of Chemical Science and Engineering, School of Chemical Engineering and Technology, Tianjin University, Tianjin, China

[6]Department of Chemical and Biomolecular Engineering, National University of Singapore, Singapore, Singapore

[7]Department of Chemical and Biomolecular Engineering, University of California Berkeley,

Berkeley, California, United States

[8]Liquid Sunlight Alliance, Lawrence Berkeley National Laboratory, Berkeley, California 94720, United States

[9]Department of Chemistry and Chemical Engineering, California Institute of Technology, Pasadena, California, United States

[10]Institute of Sustainability for Chemicals, Energy and Environment (ISCE^2), Agency for Science, Technology and Research (A*STAR), Jurong Island, Singapore

[11]Institute for Infocomm Research, Agency for Science, Technology, and Research (A*STAR), Connexis, Singapore

† These authors contributed equally to this work.

*Corresponding authors: haa@caltech.edu, lumyw@nus.edu.sg

Methods

Materials. Potassium hydroxide (ACS reagent, ≥85%), potassium formate (ReagentPlus, 99%), potassium bicarbonate (≥99.95% trace metals basis) and 8-Aminopyrene-1,3,6-trisulfonic acid trisodium salt (APTS, ≥96.0%), were purchased from Sigma-Aldrich. Nickel foam and anion exchange membrane (Fumasep FAA-3-PK-130) were purchased from Fuel Cell Store. Hydrophobic PTFE substrates of various pore sizes were obtained from Beijing Zhongxingweiye Instrument Co. Ltd. The custom designed electrochemical flow cell and Ag/AgCl (3M KCl) reference electrodes were procured from Tianjin Aida Hengsheng Technology Development Co. For confocal microscopy experiments, a leakless Ag/AgCl reference electrode from eDAQ and a Pt mesh (99.9%, 0.0726 mm diameter wires) from Alfa Aesar were used. Ltd. Aminex HPX-87H columns were used for high performance liquid chromatography and these were purchased from Bio-Rad Laboratories. The standard calibration gas mixtures for calibrating the gas chromatography system were obtained from CitiSafe Pte. Ltd. All materials were used as received without any further purification or treatment.

Fabrication of Ag/PTFE and Cu/PTFE. Samples were fabricated by sputter deposition of 325 nm Ag or Cu onto PTFE substrates of various pore sizes, using a DC sputtering system (Denton Discovery D18). The Ag and Cu sputtering targets (Latech Scientific Supply Pte. Ltd.) used both have a diameter of 3", thickness of 3 mm and a purity of 99.99%.

Materials characterization. XRD analysis of Ag/PTFE samples was carried out with a Bruker D8 Discover diffractometer using Cu Kα radiation under 40 kV and 40 mA. Catalyst morphology was studied using scanning electron microscopy (SEM) using a JEOL 7600F. For cross-section SEM images, focus ion beam (FIB) scanning electron microscopy (FEI Helios NanoLab 450) was used. Before the FIB cut can be made, each PTFE/Ag sample is first coated with 100 nm of carbon using a Leica model EM ACE200, followed by another ~15 nm of Au on top of it to prevent charging of sample during the FIB cutting process. In the FIB system, a strip of Pt of 500 nm thickness is deposited onto the desired area to be cut before starting the milling process. The sample is then milled down slowly, moving deeper into the depth of the sample until the desired SEM cross-section is achieved. A current of 2.5 nA was used for the milling process.

Electrochemical CO_2 reduction. The Ag/PTFE samples were tested in a custom designed electrochemical flow cell system (Fig. S13), with an active area of 1 cm^2 (cathode). This was operated under ambient pressure and temperature. An Autolab PGSTAT302N potentiostat system was used to control the current and measure the voltage supplied to the electrochemical cell. The potentiostat system was equipped with a FRA32M module for performing electrochemical impedance spectroscopy (EIS) measurements. In the flow cell, Ni foam was used as the counter electrode (anode) and an anion exchange membrane was used to separate the cathode and anode chambers. Ag/AgCl (3M KCl) was used as the reference electrode. $KHCO_3$ solution of varying concentrations was employed as the electrolyte used for both the catholyte and anolyte. The electrolyte was stored in external centrifuge tube reservoirs and continuously recirculated through the electrochemical cell using peristaltic pumps.

CO_2 was supplied at a flow rate of 20 sccm using a mass flow controller (Alicat Scientific) to the backside of the Ag/PTFE gas diffusion electrode. The effluent CO_2 exiting the cell was directly connected to an online gas chromatography (GC) system (Shimadzu Nexis GC-2030), for analysis of gas products. The GC was equipped with a thermal conductivity detector for analysis of H_2 and a methanizer+flame ionization detector for analysis of CO. Calibration of the GC was performed using standard calibration gas mixtures. At the end of the experiment, the formate in both the catholyte and anolyte were analyzed using high-performance liquid chromatography (Shimadzu LC-2030C NT) equipped with a UV and RID detector. Calibration was carried out by injecting known concentrations of aqueous potassium formate solutions into the system.

Double layer capacitance measurements. These were performed in the same electrochemical cell as that for CO_2R. 1 M $KHCO_3$ was employed as the electrolyte and cyclic voltammetry was carried out in a potential window where faradaic processes do not take place. This was carried out under various scan rates of 80, 60, 40 and 20 mV/s. The capacitance current density was plotted vs scan rate and the slope of this graph gives the double layer capacitance. This value is directly proportional to the electrochemically active surface area (ECSA)[1].

Confocal microscopy experiments. Confocal microscopy experiments were performed with a Zeiss LSM 880 confocal microscope (Fig. S17). A WN Achroplan 63x water immersion objective with a working distance of 1.7 mm was used. A customized electrochemical cell was designed and 3D-printed to be compatible with confocal microscopy and a water immersion objective (Fig 6a). The cell is oriented horizontally and operates without an ion exchange membrane. A rubber gasket between the gas chamber and electrolyte chamber seals the cell. The flow rate of the CO_2 gas stream through the gas chamber was adjusted to 10 sccm. The electrolyte chamber exhibits two perpendicular inlet and outlet tubes. Electrolyte is recirculated through the electrochemical cell at a flow rate of 6 mL/min. The active surface area of the working electrode is 0.2 cm^2. A leakless Ag/AgCl reference electrode and a Pt mesh counter electrode are both immersed into the electrolyte. 200 µM APTS was dissolved in 1 M $KHCO_3$ electrolyte and filled into the electrolyte chamber. A 458 nm laser scans the sample and excites the fluorescent APTS dye molecules. The laser power is set to 100%, the pinhole to 57.1 µm and the gain to 800. The emission is collected separately in the wavelength intervals 480 – 550 nm and 551 – 754 nm. The ratio between the two signals collected is a measure of the local pH value. The pH value can be calculated with a previously determined sigmoidal calibration curve:

$$pH = \frac{1}{2.743} ln\left(-1 + \frac{5.005}{(Ratio\ of\ Emission)_{APTS} - 0.1041}\right) - 11.95.$$

More details about the calibration of APTS can be found elsewhere[2]. Before each experiment, a potentiostatic electrochemical impedance spectroscopy (PEIS) was performed with a Biologic SP-200 potentiostat to determine the solution resistance of the cell. A constant current was then applied with the potentiostat while performing an automatic 85% IR electronic compensation of the electrochemical potential. The system was allowed to equilibrate for 15 seconds before taking fluorescence measurements. The laser beam scanned the electrolyte in the vicinity of the electrode in the plane perpendicular to the electrode surface by scanning the laser line by line and moving the stage in the z-direction in 0.5 µm increments. The first line was placed a few micrometers below the electrode surface. The dimensions of the resulting map are 120 µm in x and 50 µm in z. The measuring speed was adjusted so that capturing one frame takes approximately 30 seconds. In between measurements, the electrolyte was removed from the electrochemical cell and replaced with electrolyte containing fresh APTS. Each measurement was performed at least six times.

Multiphysics simulations. The model employed was previously reported by Weng et al. and full details can be found in the corresponding publication[3]. The simulations were implemented using COMSOL Multiphysics software. This model is a stationary, isothermal and 1D axisymmetric model for the cathodic compartment of the cell, which contains the nanoparticle Ag catalyst layer and diffusion medium. CO formation and hydrogen evolution reaction are the two electrochemical reactions focused on. Triangular meshes were applied.

The governing equation is mass balance, which is written as

$$R_i = \nabla \cdot n_i = \nabla \cdot J_i + u \cdot \nabla c_i$$

where R_i is reaction rate, n_i is mass flux, J_i is diffusive mass flux, u is velocity and c_i is concentration.

For charged chemical species in liquid phase, the Nernst–Planck equation is the conservation of mass equation. With assumption that the convection is negligible, the equation can be written as:

$$n_i = -D_i \nabla c_i - z_i u_{m,i} F c_i \nabla \varphi_l$$

where D_i is the diffusivity of the chemical species, z_i is the valence of ionic species, $u_{m,i}$ is the mobility in medium m, F is the Faraday's constant, and φ_l is the potential of liquid phase.

The reaction rate is composed of three elements,

$$R_i = R_{ec,i} + R_{dis,i} + R_{b,i}$$

where $R_{ec,i}$, $R_{dis,i}$ and $R_{b,i}$ represents electrochemical reaction, CO_2 dissolution and homogeneous bulk reactions respectively.

For each electrochemical reaction, the reaction rate is:

$$R_{ec,i,k} = -\frac{\nu_i a_v i_k}{nF}$$

where ν_i is stoichiometric number, a_v is specific surface area and n is electron transferred in reaction. i_k is current density of reaction k, which is calculated by the generic concentration dependent Butler-Volmer type kinetics,

$$i_k = -i_{0,k} C_O \exp\left(-\frac{\alpha_{c,k} F}{RT} \eta_k\right)$$

where is C_O dimensionless concentration, $i_{0,k}$ is exchange current density and $\alpha_{c,k}$ is cathodic charge transfer coefficient. The overpotential η_k is:

$$\eta_k = \varphi_s - \varphi_l - (U_{0,k} - 0.059pH)$$

where $U_{0,k}$ is reference potential and φ_s is the potential of gas phase. Moreover, for electrochemical reactions, the process is governed by charge conservation and Ohm's law as well,

$$\nabla \cdot i_s = -\nabla \cdot i_l = a_v \sum_k i_k$$

$$i_s = -\sigma_s \nabla \varphi_s$$

where σ_s is the electrical conductivity. Here, Bruggeman relationship is applied to obtain the effective σ_s as the diffusion medium is porous.

The dissolution rate of CO_2 is obtained by Fick's law:

$$R_{dis,CO_2} = \frac{D_{CO_2(l)} a_v \Delta p}{\delta_{TF}}$$

where Δp is difference in CO_2 partial pressure across the thin electrolyte film with thickness δ_{TF}.

The homogenous buffering reactions are mainly carbonate and water dissociation reactions:

$$R_{B,i,k} = k_n \prod_{\nu_i < 0} c_i - k_{-n} \prod_{\nu_i > 0} c_i$$

where k_n and k_{-n} are rate constants for forward and reverse homogeneous reaction.

For gas phase, the mass flux is composed of diffusion and convection:

$$n_i = j_i + \rho_i u_g$$

where ρ_i is gas density.

The reactions in the gas phase only includes electrochemical reactions and CO_2 dissolution.

$$R_i = R_{ec,i} + R_{dis,i}$$

$$R_{dis,CO_2} = -\frac{D_{CO_2(l)} a_v \Delta p}{\delta_{TF}}$$

$$R_{ec,i,k} = -\frac{\nu_i a_v i_k}{nF}$$

The diffusive flux j_i is calculated using a mixture averaged diffusion model,

$$j_i = -\rho_i D_i^{eff} \nabla \omega_i - \rho_i D_i^{eff} \omega_i \frac{\nabla M_n}{M_n}$$

where ω_i is mass fraction, M_n is the average molar mass of gas mixture. The effective diffusion coefficient is corrected by Bruggeman correlation.

The model was validated under various potential ranging from -0.8 to -2.0 V vs RHE. The order of magnitude of calculated current densities is similar to reference based on experimental data and shows similar tendency along with the change of applied potential.

For the purposes of this work, the porosity values of the diffusion media and catalyst layer were set to be identical to each other and varied across the values of 0.4, 0.5, 0.6, 0.7 and 0.8. A parametric sweep was used to facilitate this simulation process. The CO_2 concentration and pH profile were determined for each porosity value, at cathodic current densities of 100, 200, 300, 400 and 500 mA/cm^2.

List of symbols used in the model:

$\alpha_{c,k}$ Cathodic charge transfer coefficient

Δp Difference in CO_2 partial pressure across the thin electrolyte film with thickness, atm

δ_{TF} Thin electrolyte film thickness

η_k Overpotential

ν_i Stoichiometric number

ρ_i Density, g/cm^3

σ_s Electrical conductivity, S/m

φ_l Potential of liquid phase, V

ω_i Mass fraction

a_v Specific surface area, 1/m

C_O Dimensionless concentration

c_i Concentration, mol/m^3

D_i Diffusivity, m^2/s

F Faraday's constant, C/mol

i Current density, mA/cm^2

$i_{0,k}$ Exchange current density, mA/cm^2

J_i Diffusive mass flux, m^2/s

k_n, k_{-n} Rate constants for forward and reverse homogeneous reaction

M_n Average molar mass of gas mixture, g/mol

n Numbers of electron transferred in reaction

n_i Mass flux, g/(m^2·s)

R_i Reaction rate, g/(m^3·s)

u Velocity, m/s

$u_{m,i}$ Mobility in medium m, s/(mol·kg)

$U_{0,k}$ Reference potential, V

z_i Valence of ionic species

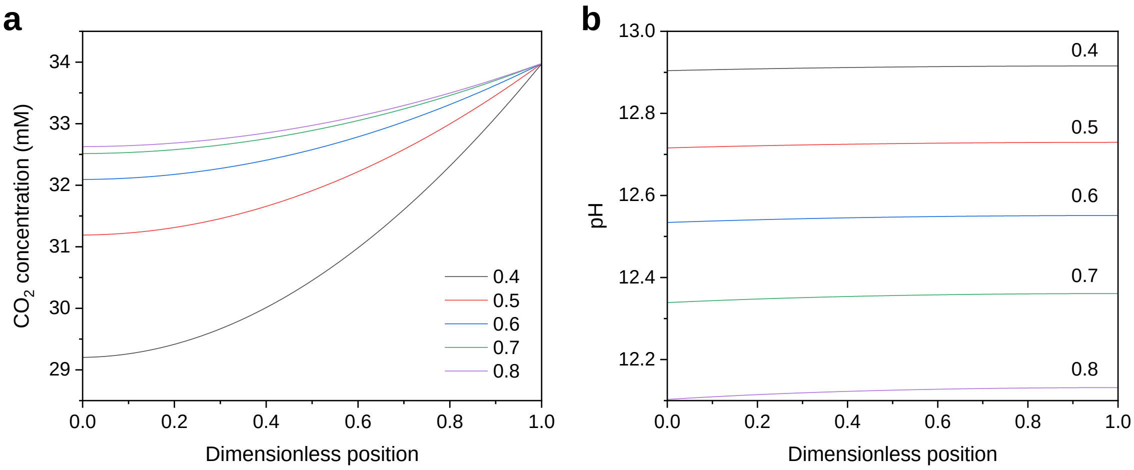

Fig. S1. Simulated (a) CO2 concentration and (b) pH profile in the boundary layer at various GDL porosity values. Applied cathodic current density is 100 mA/cm^2.

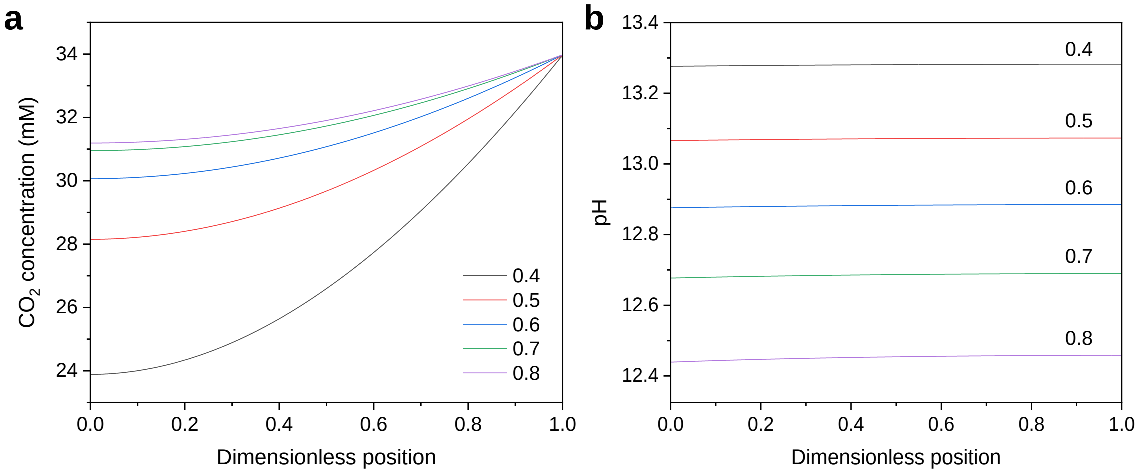

Fig. S2. Simulated (a) CO2 concentration and (b) pH profile in the boundary layer at various GDL porosity values. Applied cathodic current density is 200 mA/cm^2.

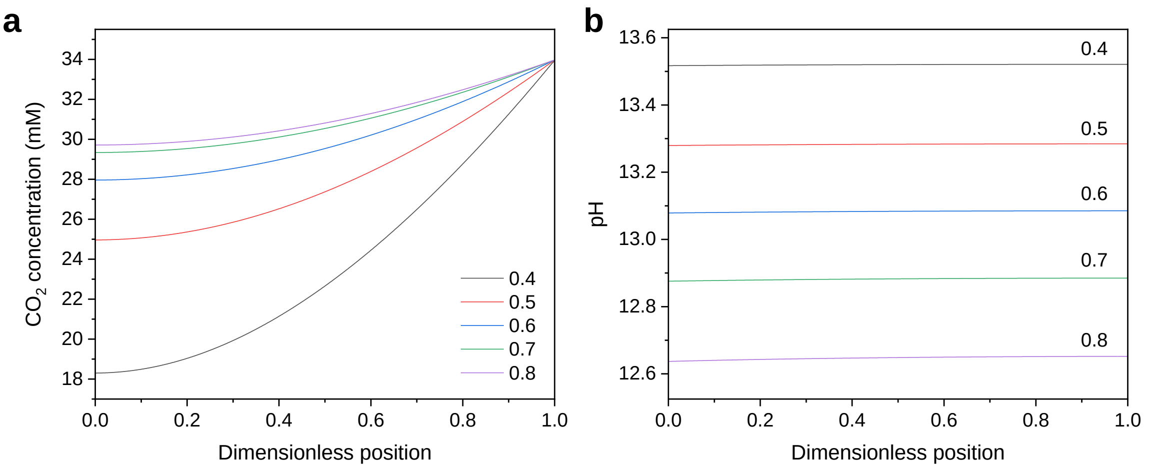

Fig. S3. Simulated (a) CO_2 concentration and (b) pH profile in the boundary layer at various GDL porosity values. Applied cathodic current density is 300 mA/cm^2.

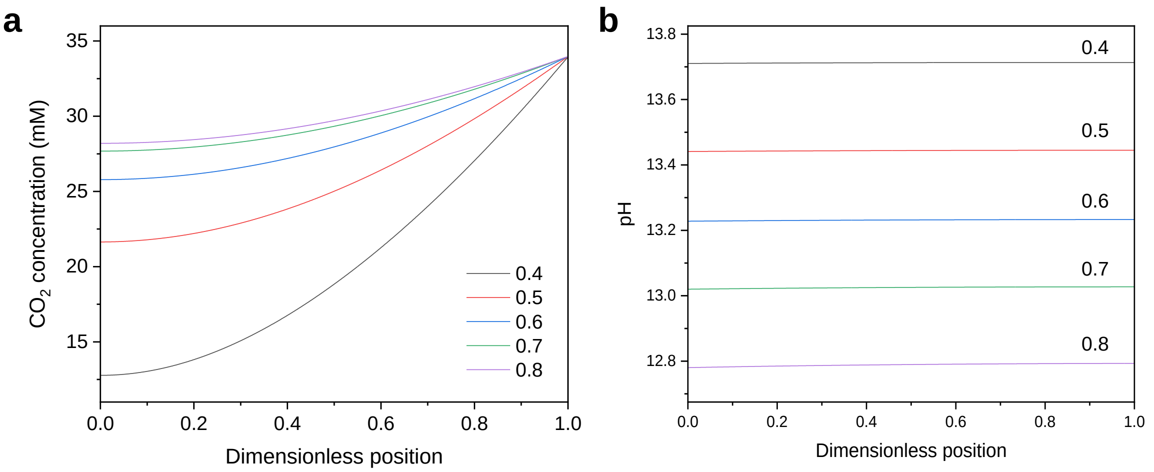

Fig. S4. Simulated (a) CO_2 concentration and (b) pH profile in the boundary layer at various GDL porosity values. Applied cathodic current density is 400 mA/cm^2.

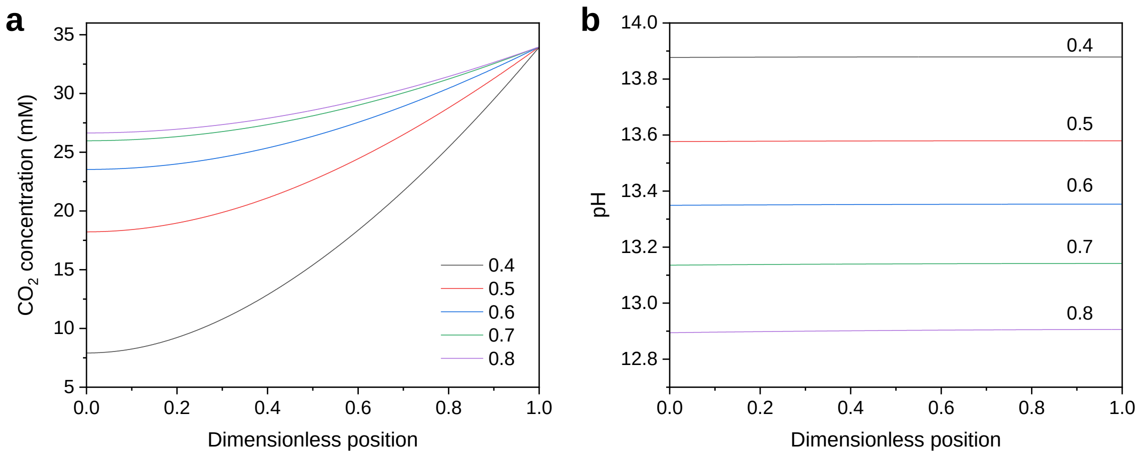

Fig. S5. Simulated (a) CO$_2$ concentration and (b) pH profile in the boundary layer at various GDL porosity values. Applied cathodic current density is 500 mA/cm^2.

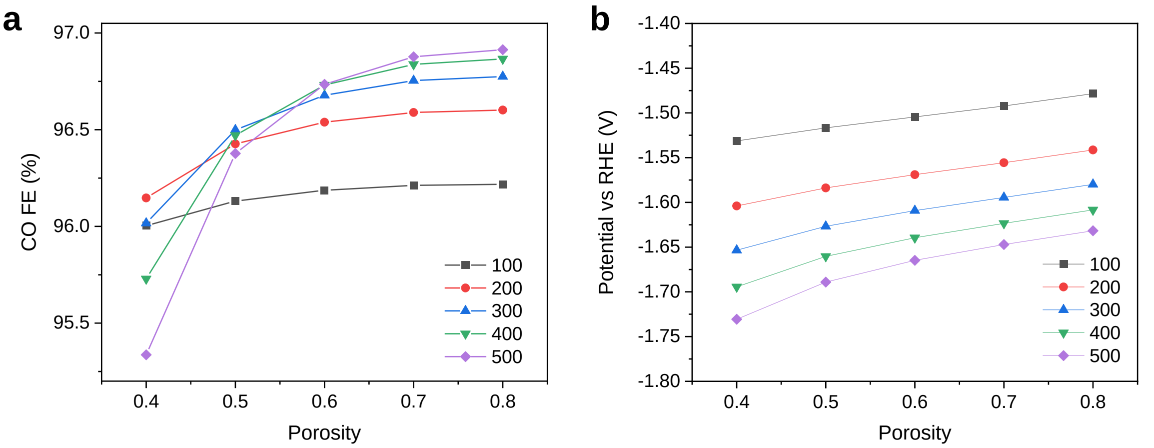

Fig. S6. Simulated (a) CO FE and (b) applied potential at various GDL porosity values. The values in the legends of both figures are current densities with units of mA/cm^2.

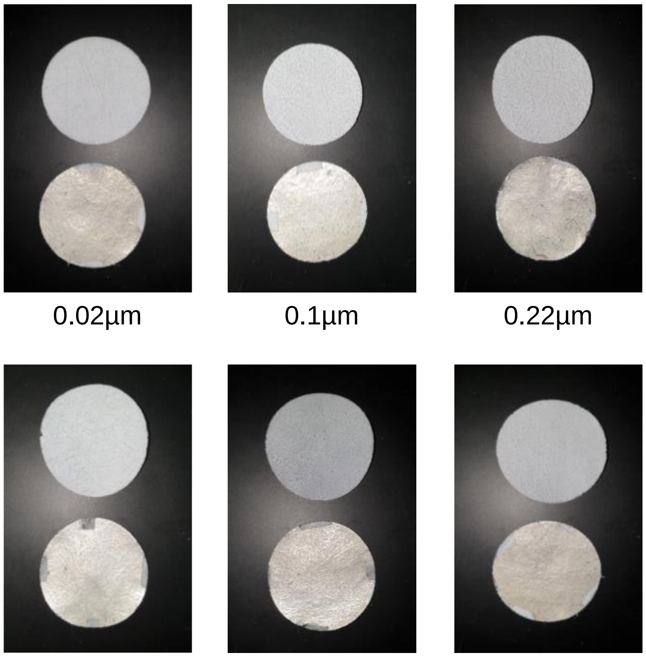

0.02µm 0.1µm 0.22µm

0.45µm 1.0µm 3.0µm

Fig. S7. Digital photographs of pristine and Ag sputter coated PTFE substrates for each pore size. For each pore size, the pristine case is placed on top and the coated case is placed at the bottom.

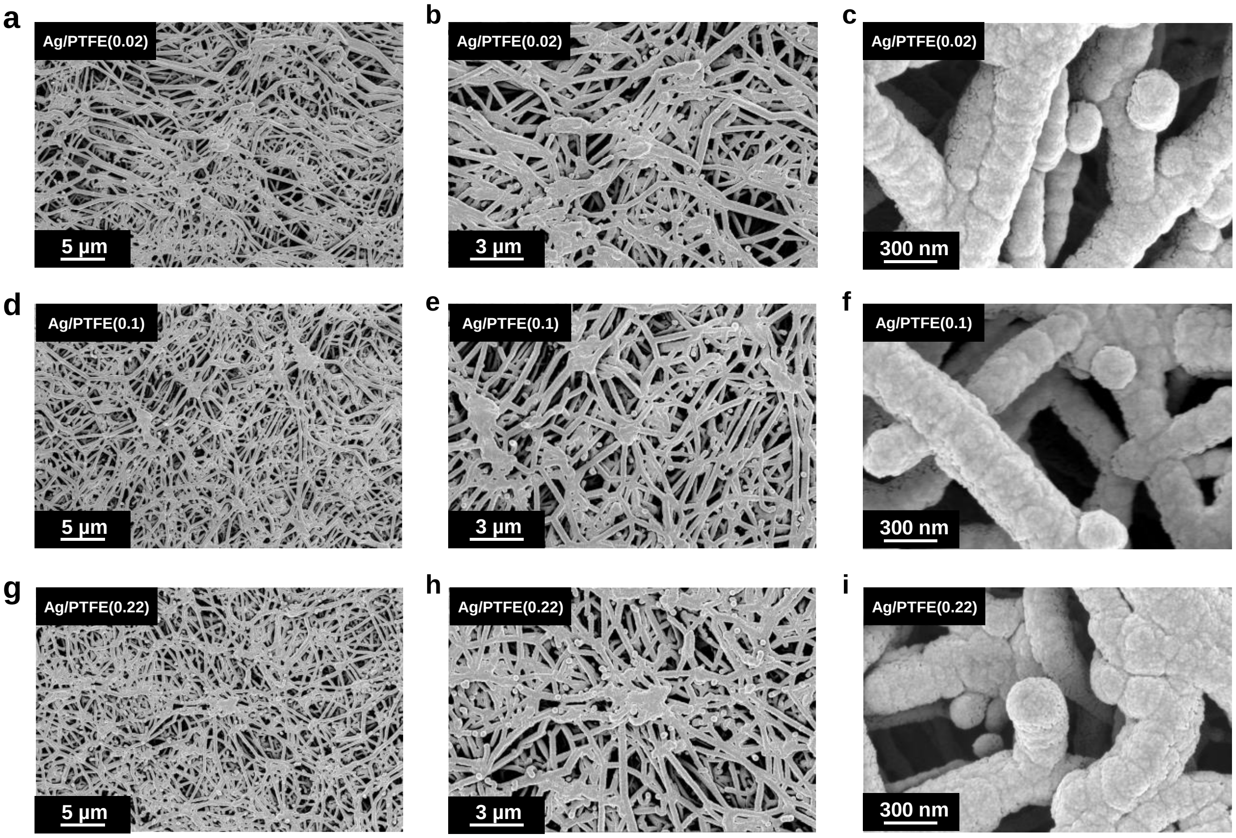

Fig. S8. Top-down SEM images of Ag/PTFE with different magnifications. (a), (b) and (c) are for Ag/PTFE(0.02). (d), (e) and (f) are for Ag/PTFE(0.1). (g), (h) and (i) are for Ag/PTFE(0.22)

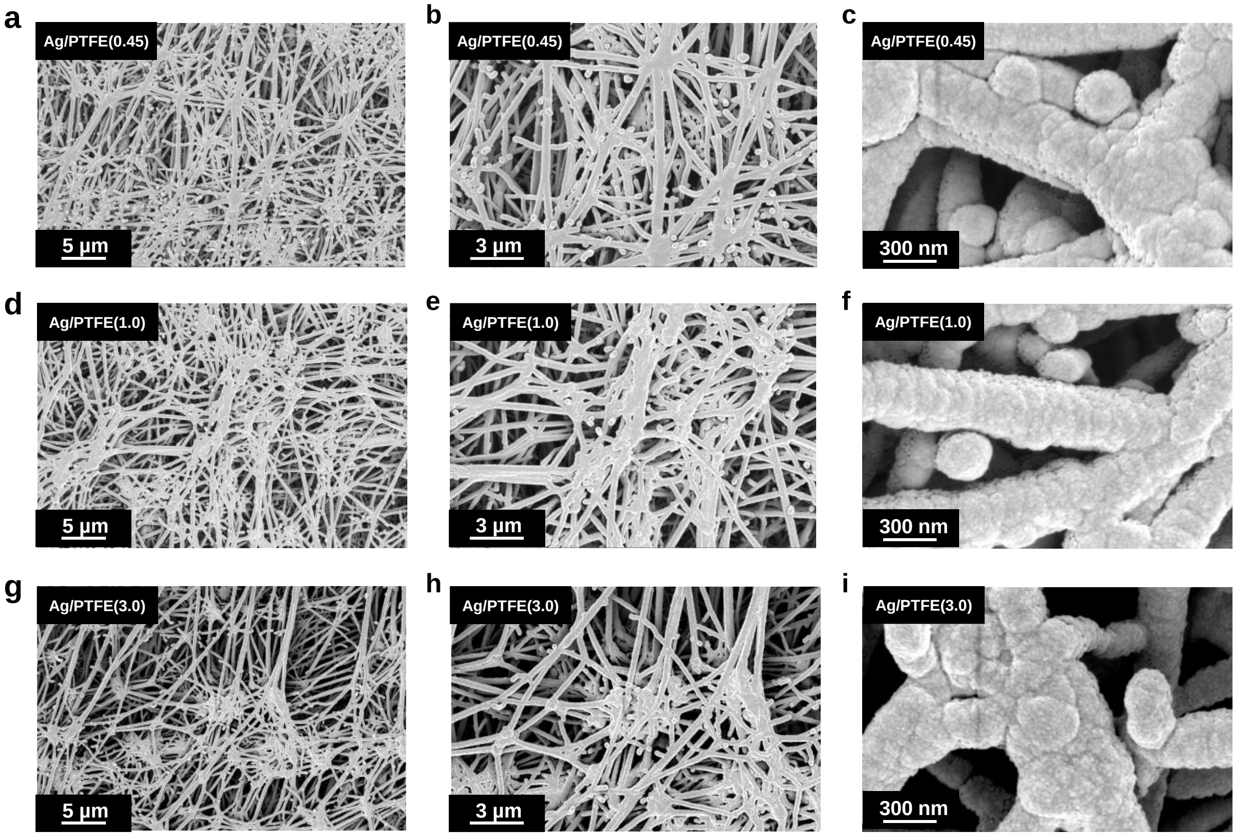

Fig. S9. Top-down SEM images of Ag/PTFE with different magnifications. (a), (b) and (c) are for Ag/PTFE(0.45). (d), (e) and (f) are for Ag/PTFE(1.0). (g), (h) and (i) are for Ag/PTFE(3.0)

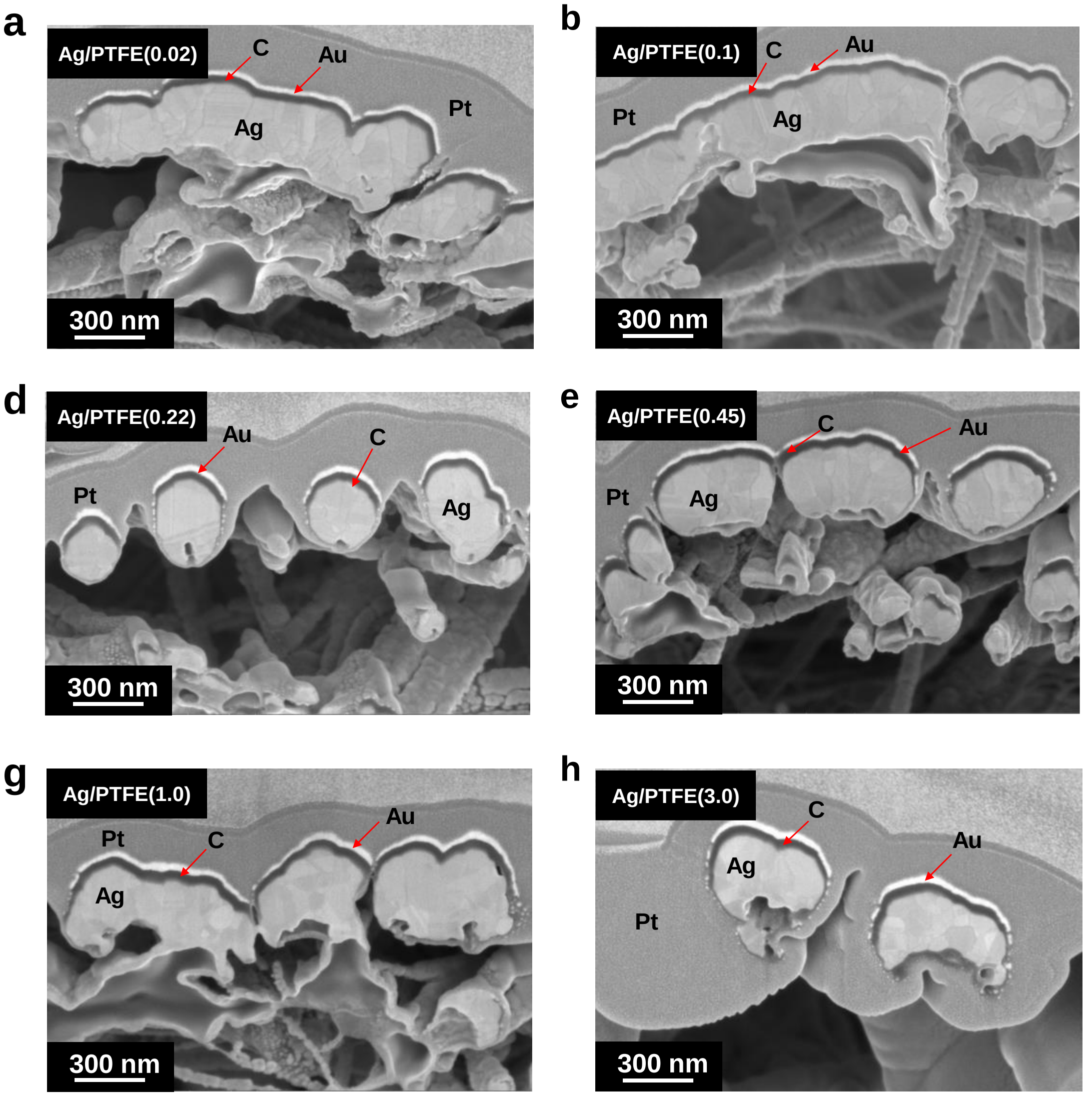

Fig. S10. Cross-section SEM images of (a) Ag/PTFE(0.02), (b) Ag/PTFE(0.1), (c) Ag/PTFE(0.22), (d) Ag/PTFE(0.45), (e) Ag/PTFE(1.0) and (f) Ag/PTFE(3.0). See methods section for a description of the preparation process.

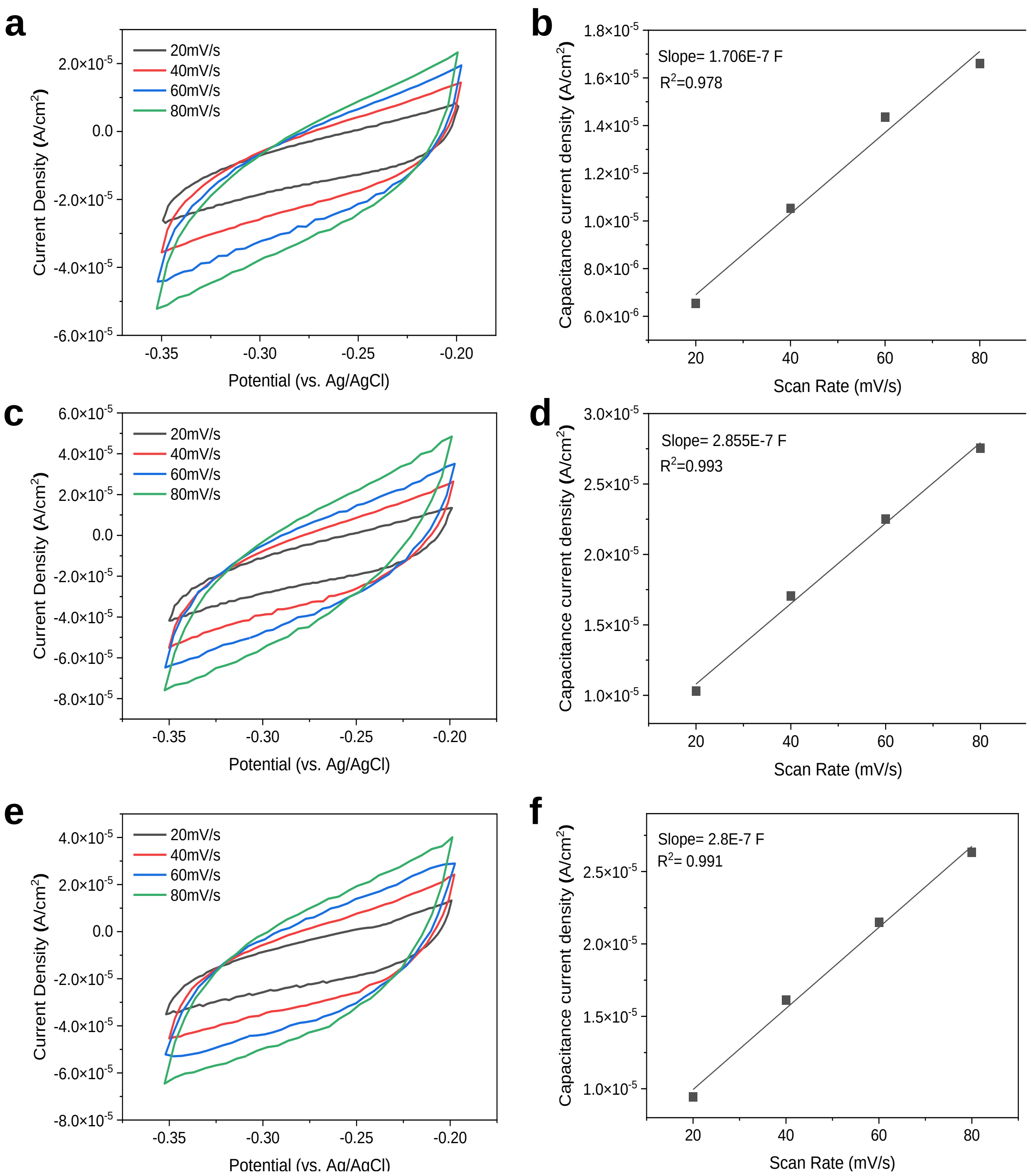

Fig. S11. (a), (c) and (e) are cylic voltammetry results at various scan rates for Ag/PTFE(0.02), Ag/PTFE(0.1) and Ag/PTFE(0.22) respectively. (b), (d) and (f) are the capacitance current density plotted against the scan rate for for Ag/PTFE(0.02), Ag/PTFE(0.1) and Ag/PTFE(0.22) respectively. The slope of the graph gives the capacitance, which is directly proportional to the electrochemically active surface area (ECSA).

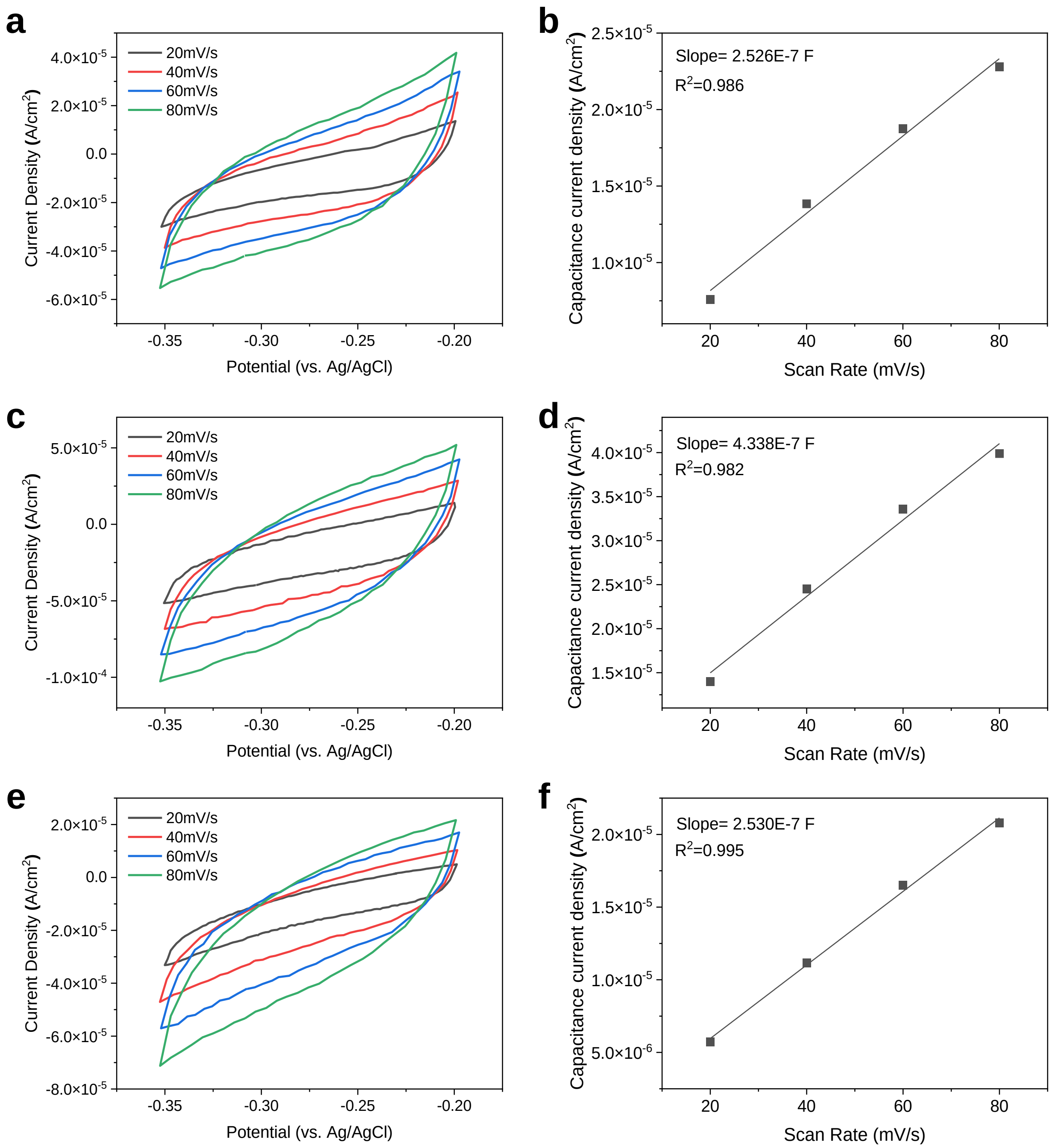

Fig. S12. (a), (c) and (e) are cylic voltammetry results at various scan rates for Ag/PTFE(0.45), Ag/PTFE(1.0) and Ag/PTFE(3.0) respectively. (b), (d) and (f) are the capacitance current density plotted against the scan rate for for Ag/PTFE(0.45), Ag/PTFE(1.0) and Ag/PTFE(3.0) respectively. The slope of the graph gives the capacitance, which is directly proportional to the electrochemically active surface area (ECSA).

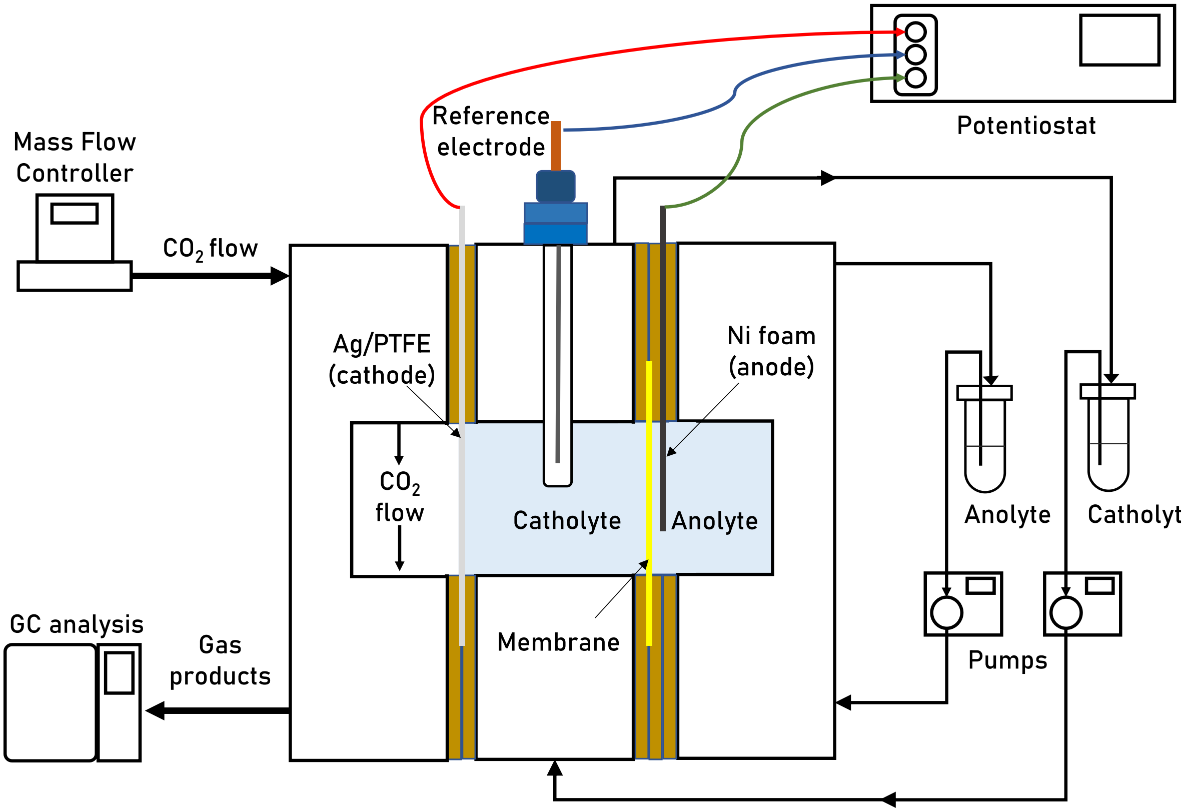

Fig. S13. Schematic of the experimental setup used to perform electrochemical CO_2 reduction. A flow type system is employed, with the catholyte and anolyte continuously recirculated through the cell from an external reservoir using peristaltic pumps. Gas products are analyzed using a gas chromatograph and formate is analyzed using liquid chromatography. Note: items in the schematic are not drawn to scale.

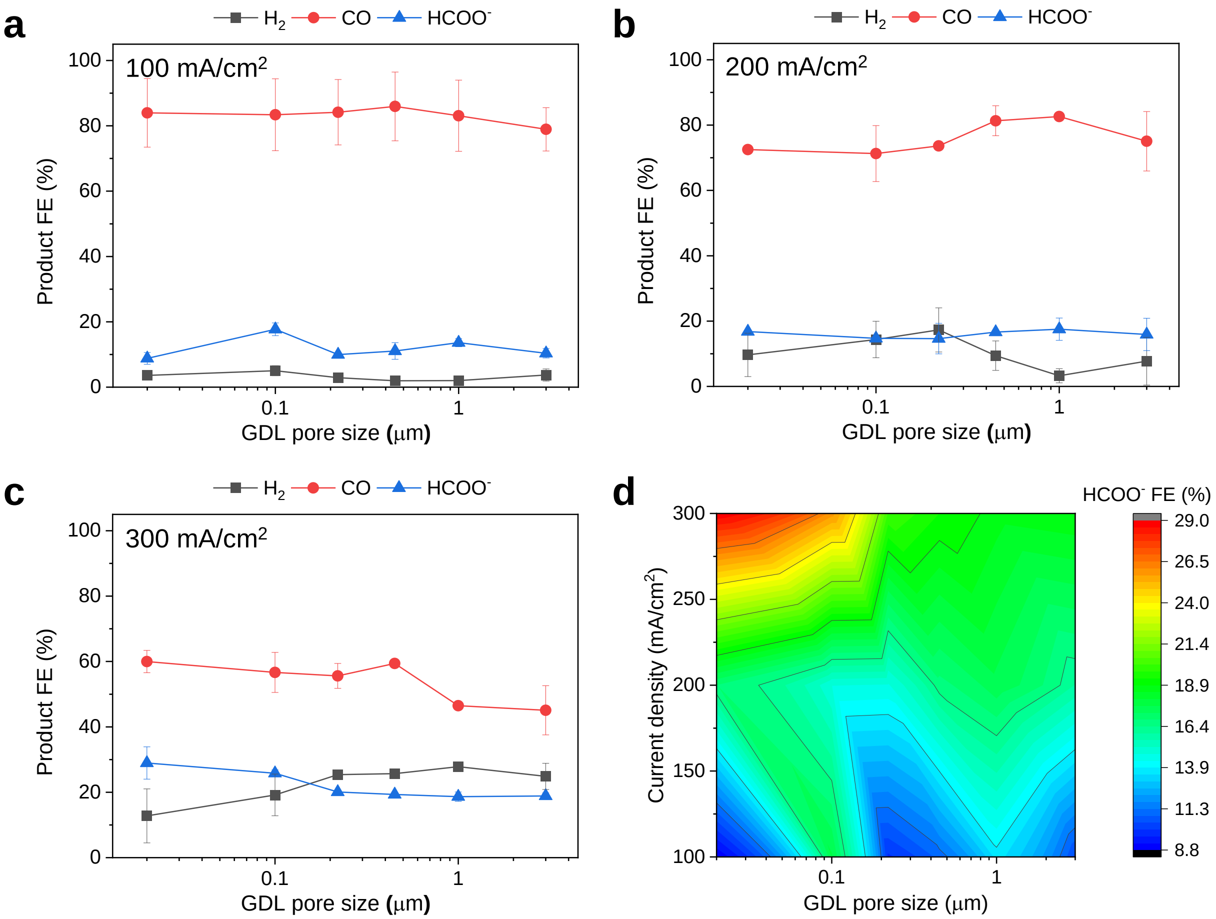

Fig. S14. Electrochemical CO_2 reduction FE results with 2 M $KHCO_3$ as the electrolyte. (a), (b) and (c) show the product FE data for Ag/PTFE as a function of GDL pore size under cathodic current densities of 100, 200 and 300 mA/cm^2 respectively. (d) is the corresponding color contour map of the $HCOO^-$ FE data for Ag/PTFE as a function of current density and GDL pore size.

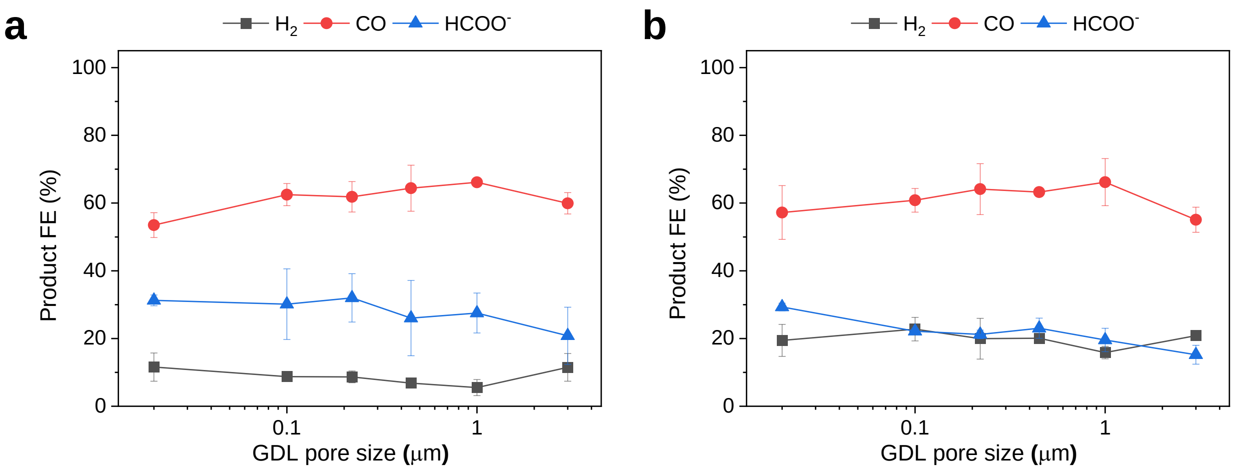

Fig. S15. Product FE data for Ag/PTFE as a function of GDL pore size at a cathodic current density of 300 mA/cm^2 in (a) 0.5 M $KHCO_3$ and (b) 1.5 M $KHCO_3$ electrolyte.

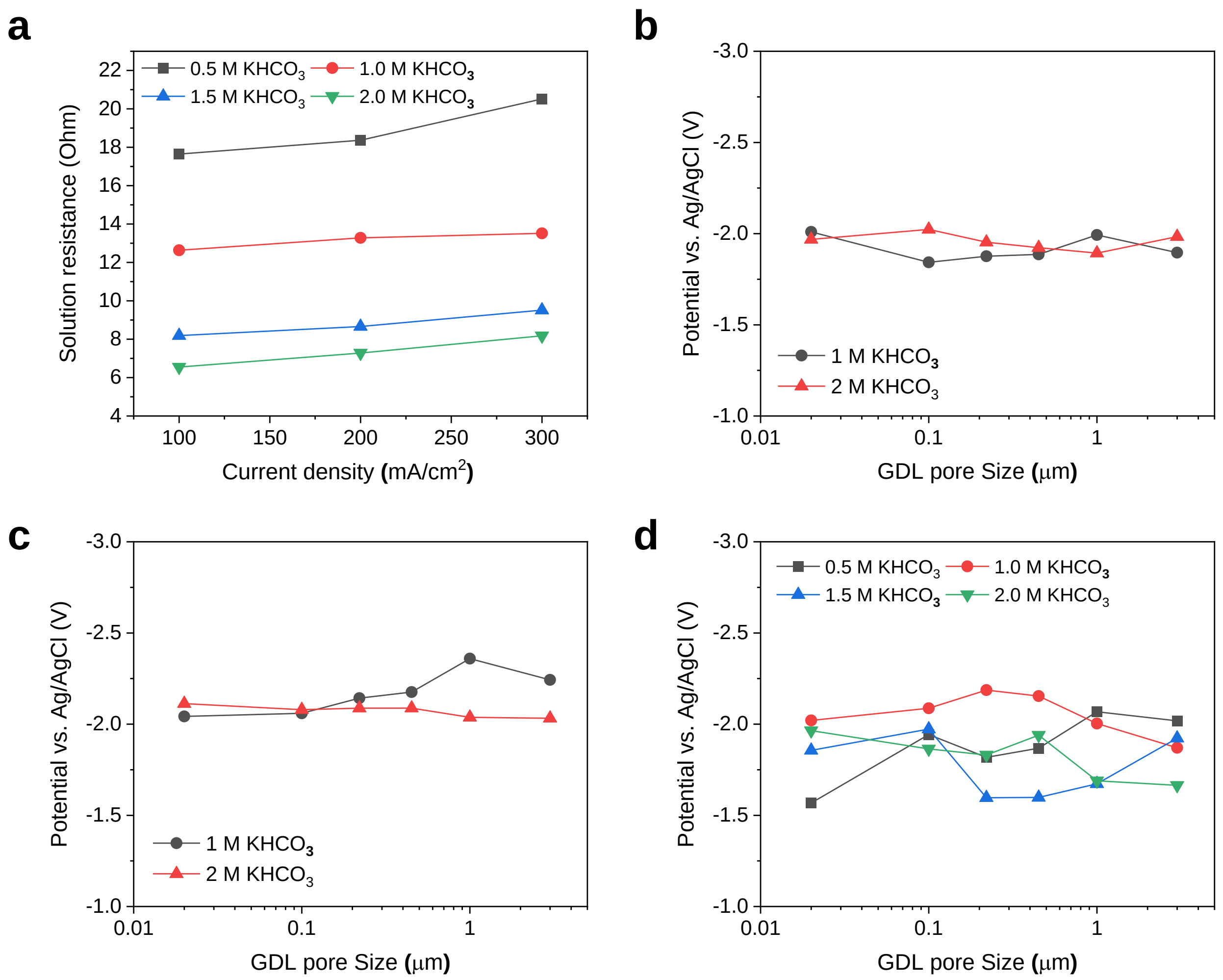

Fig. S16. (a) Solution resistance measured using electrochemical impedance spectroscopy (EIS) at various applied current densities. (b), (c) and (d) are the applied potentials (after IR correction) as a function of GDL pore size for the different buffer concentrations at cathodic current densities of 100, 200 and 300 mA/cm^2 respectively.

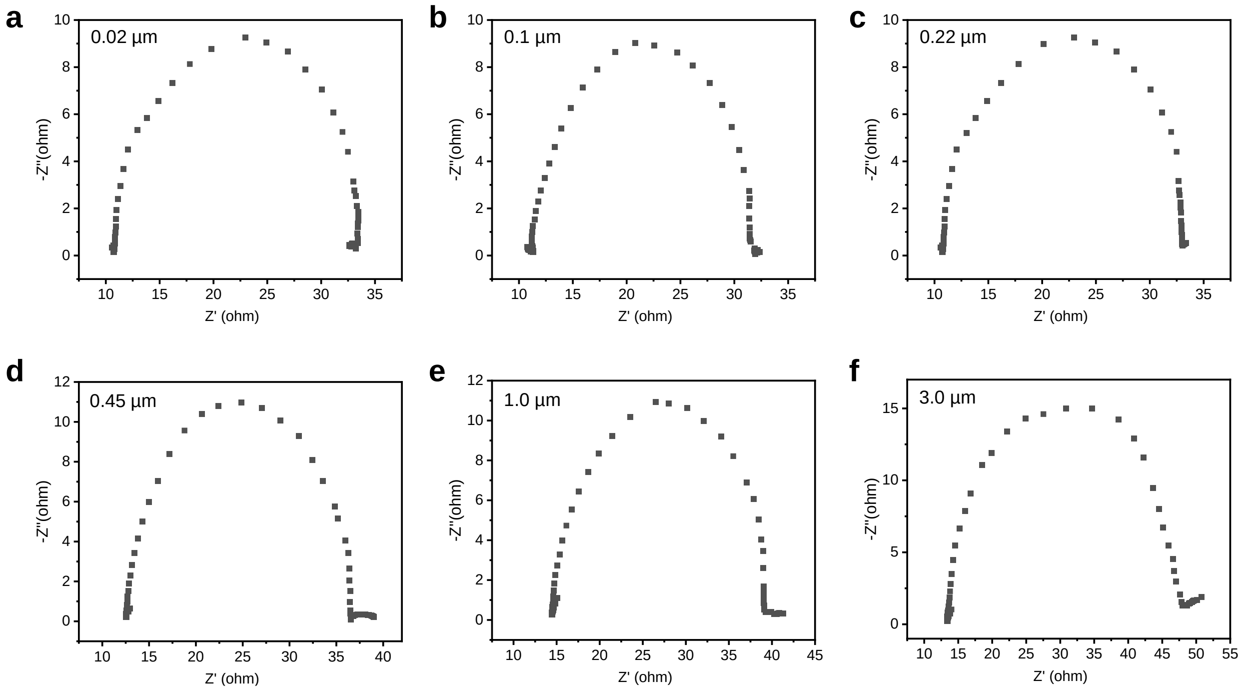

Fig. S17. Electrochemical impedance spectroscopy (EIS) measurements for the different Ag/PTFE(X) samples: (a) Ag/PTFE(0.02), (b) Ag/PTFE(0.1), (c) Ag/PTFE(0.22), (d) Ag/PTFE(0.45), (e) Ag/PTFE(1.0) and (f) Ag/PTFE(3.0).

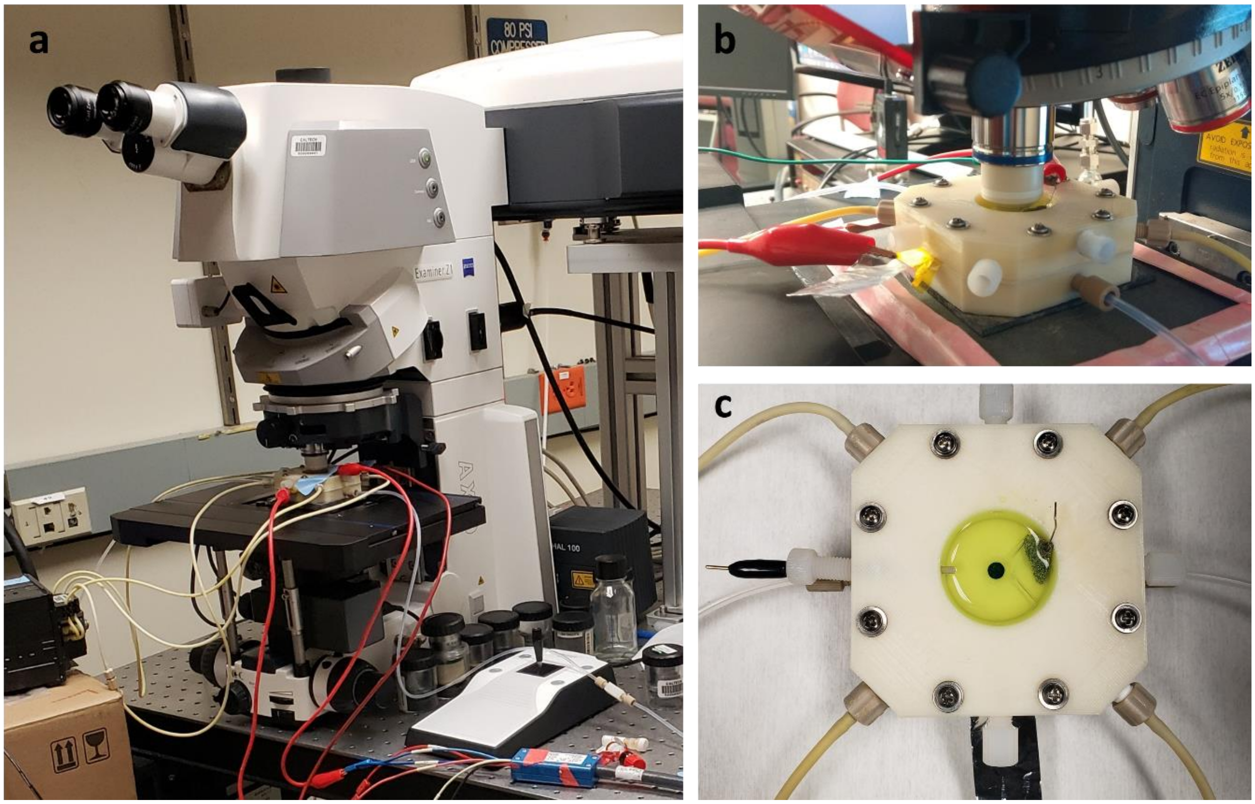

Fig. S18. Photographs of the confocal microscopy setup used to map the local pH value. (a) Zeiss LSM 880 confocal microscope with a 63x water immersion objective and an electrochemical flow cell. (b) Close-up image of the electrochemical cell. (c) Top view of the electrochemical cell, filled with APTS-spiked electrolyte.

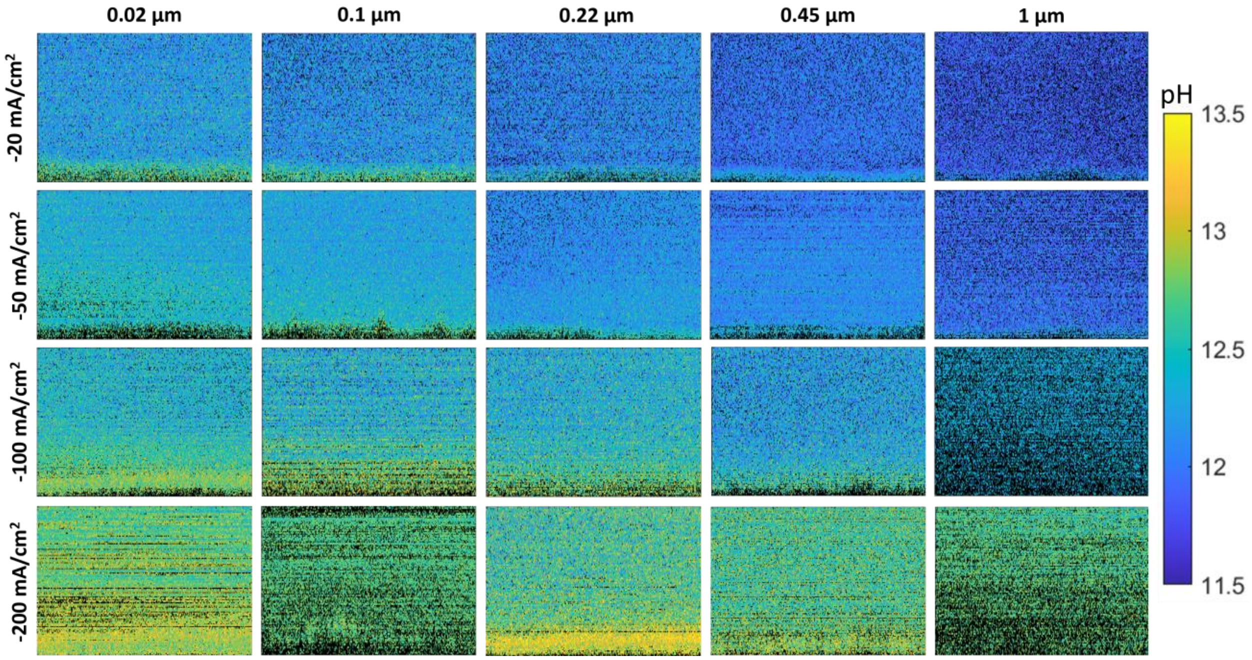

Fig. S19. Representative pH maps as a cross section through the plane perpendicular to the electrode surface for different Ag/PTFE samples at four different cathodic current densities between 20 mA/cm^2 and 200 mA/cm^2. The dimension of each of the maps is 120 µm in x and 50 µm in z.

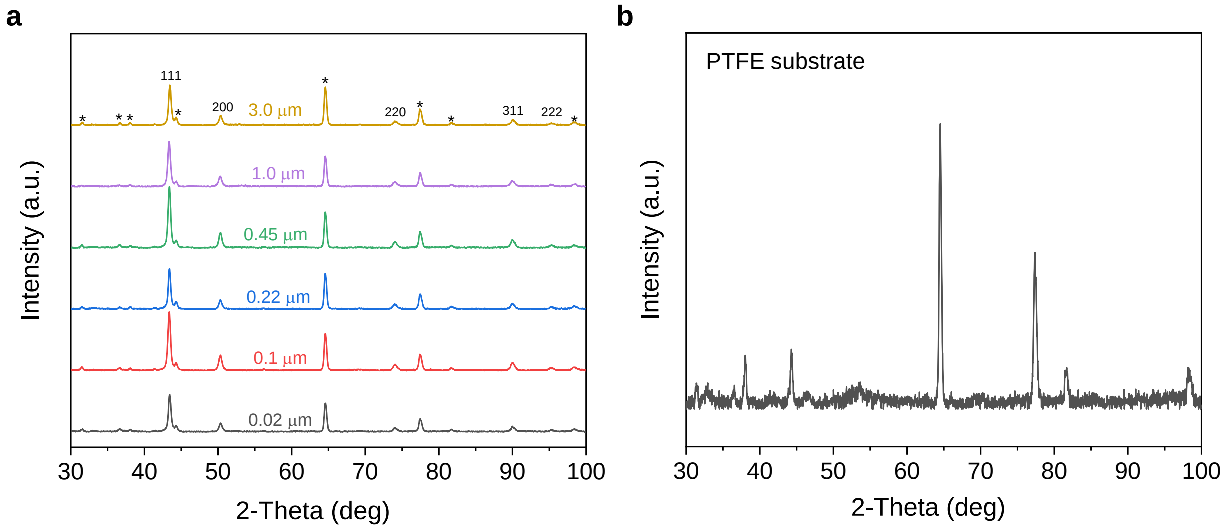

Fig. S20. (a) XRD spectrums of Cu sputtered onto PTFE substrates with various pore sizes. The peaks labelled with a (*) correspond to that of the underlying PTFE substrate. (b) XRD spectrum of the bare pristine PTFE substrate.

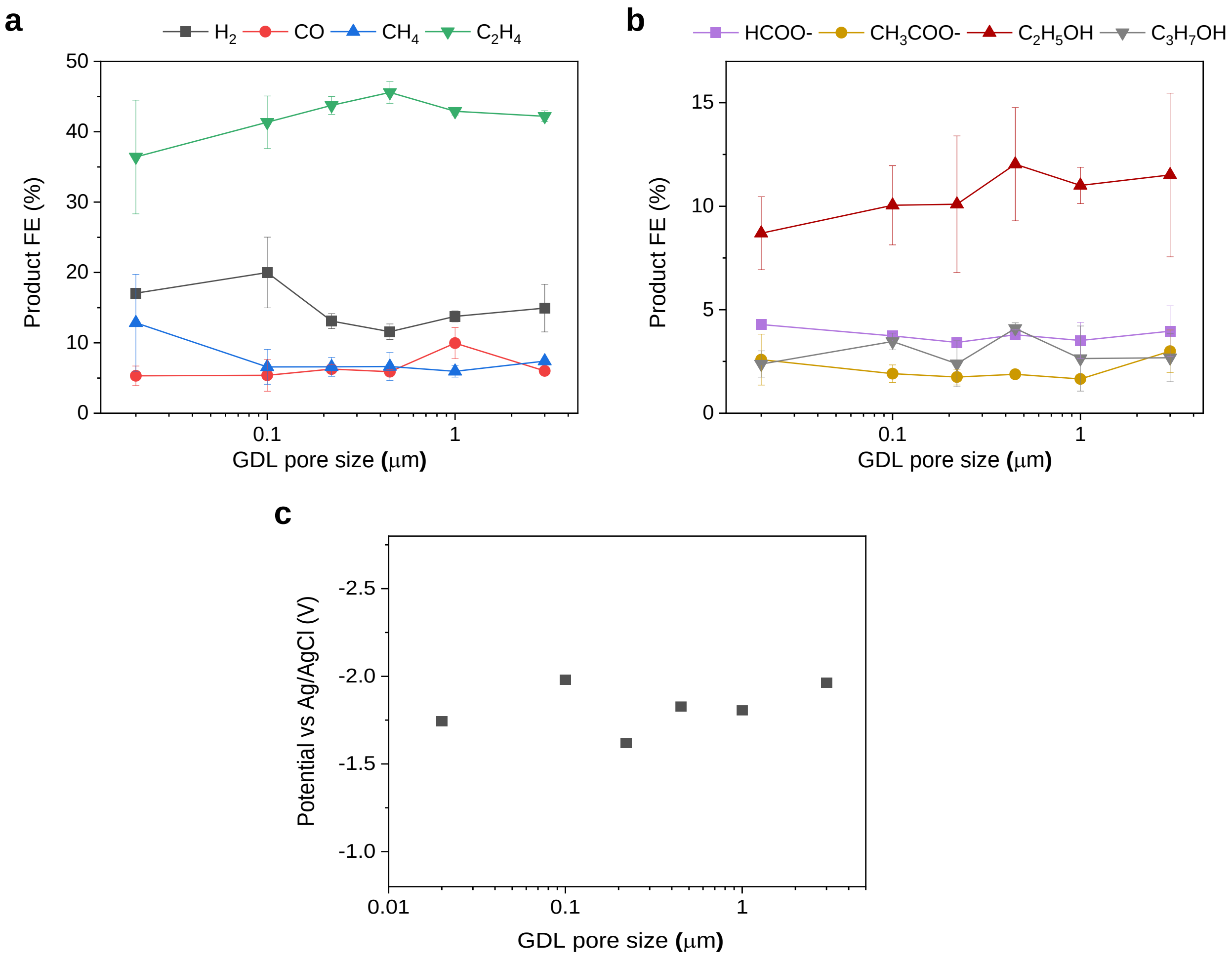

Fig. S21. Electrochemical CO_2 reduction results with Cu sputtered on PTFE substrates of various pore sizes. A constant cathodic current density of 200 mA/cm^2 was applied and 1 M $KHCO_3$ was used as the electrolyte. Multicarbon (C_{2+}) products are ethylene (C_2H_4), acetate (CH_3COO^-), ethanol (C_2H_5OH) and 1-propanol (C_3H_7OH). (a) Gas product FE as a function of pore size. (b) Liquid product FE as a function of pore size. (c) Applied potential as a function of pore size.

References

1. Clark, E. L. *et al.* Standards and Protocols for Data Acquisition and Reporting for Studies of the Electrochemical Reduction of Carbon Dioxide. *ACS Catal* **8**, 6560–6570 (2018).

2. Böhme, A. *et al.* Direct observation of the local microenvironment in inhomogeneous CO $_2$ reduction gas diffusion electrodes *via* versatile pOH imaging. *Energy Environ Sci* **16**, 1783–1795 (2023).

3. Weng, L. C., Bell, A. T. & Weber, A. Z. Modeling gas-diffusion electrodes for CO2 reduction. *Physical Chemistry Chemical Physics* **20**, 16973–16984 (2018).